AIAA-2014-1928049

AIAA Propulsion and Energy Forum and Expositions 2014
28-30 July 2014, Cleveland, Ohio, Cleveland Medical Mart & Convention Center

AIAA-2014-1928049

ON THE COMPUTATIONS OF THERMAL BEHAVIOUR OF SHELL AND TUBE HEAT EXCHANGER

Mahmoud Galal Yehia
Research Student of Mechanical Engineering, Shoubra Faculty of Engineering, Benha University
Cairo, Egypt
medogalal@yahoo.com

Ahmed A. A. Attia
Ass. Prof. of Mechanical Engineering, Shoubra Faculty of Engineering, Benha University
Cairo, Egypt
ahmed.attia@feng.bu.edu.eg

Osama Ezzat Abdelatif
Prof. of Mechanical Engineering, Shoubra Faculty of Engineering, Benha University
Cairo, Egypt
osama.abdellatif@feng.bu.edu.eg

Essam E. Khalil
Prof. of Mechanical Engineering, Cairo University
Cairo, Egypt
khalile1@asme.org

ABSTRACT

In the present research, numerical simulations of the turbulent, three-dimensional fluid flow, heat transfer, and friction for shell and tube heat exchanger using ANSYS FLUENT CFD technique are performed. The studied parameters are Nusselt number and friction factor at different values of mass flow rates (from 0.5 kg/s to 2.0 kg/s of water fluid flow) with the corresponding effect on thermal enhancement factor, and a correlation relating heat transfer and friction for different vane swirlers diameters and blade angles have been developed.

The investigated cases are the case of plain tubes and different cases with inserted vane swirlers of different blade angles (15º, 20º, 30º, 35º, 40º, 45º and 60º) and swirler diameters (5, 10, 15, 18, and 19 mm). The results showed that the highest achieved heat transfer enhancement is for φ = 19 mm and θ = 15º case, resulting in for Nusselt number, friction factor, and thermal enhancement factor times that of plain tubes case of 1.62, 58.75, and 0.42, respectively. Also, the margin for selecting the proper vane swirler is the required heat transfer enhancement level with the maximum permissible friction loss.

Throughout the investigation; numerical validation is carried out by comparing the numerical predictions obtained from the present model with the results reported in the literature. Fair agreement is found among both results.

Keywords: numerical simulation, shell and tube heat exchanger, turbulence model, vane swirler.

NOMENCLATURE

A	Area (m^2)
c_p	Pressure coefficient (J/kg.K)
C_v	Constant
$C_{1\varepsilon}$	Constant
$C_{2\varepsilon}$	Constant
D	Diameter (m)
D_b	Propeller diameter (m)
D_p	Pipe diameter (m)
f	Friction factor
G_b	Generation of turbulent kinetic energy due to buoyancy (m^2/s^2)
G_k	Turbulent kinetic energy production (m^2/s^2)
h	Heat transfer coefficient ($W/m^2.K$)
h_i	Heat transfer coefficient for pure cross flow in ideal tube bank ($W/m^2.K$)
I	Turbulence intensity (%)
J_b	Bypass correction factor, tube bundle to shell
J_c	Segmental baffle window correction factor
J_l	Baffle leakage correction factor
J_r	Laminar heat transfer correction factor, applicable for Re < 100
J_s	Unequal inlet/outlet baffle spacing correction factor, applicable only if such differences exist
k	Turbulence kinetic energy (m^2/s^2)
L	Length (m)
L_p	Pipe length (m)
L_t	Inter-turbulator distance (m)

$\dot{m}$	Mass flow rate (kg/s)
na	Constant
Nu	Nusselt number
p	Pressure (pa)
Pr	Prandtl number
Re	Reynolds number
T	Temperature (K)
TEF	Thermal enhancement factor
S_k	User-defined source term
S_ε	User-defined source term
t	Time (s)
U	The mean velocity near the wall region (m/s)
Y_M	The dilatation dissipation term
x, y, z	Cartesian coordinate Components
u, v, w	Instantaneous velocity component in x, y, z directions
Δp	Pressure drop (pa)
Δp_c	Combined pressure drop of all the interior cross flow section (baffle tip to baffle tip) (pa)
Δp_e	Pressure drop in the two end zones (pa)
Δp_w	Combined pressure drop in all the windows crossed (pa)
ΔT	Temperature difference (K)
α_k	Inverse effective Prandtl numbers for the dissipation
ε	Turbulence dissipation rate (m^2/s^3)
θ	Blade angle (^{o})
κ	Thermal conductivity coefficient (W/m.K)
μ	Dynamic viscosity ($N.s/m^2$)
ρ	Density (kg/m^3)
φ	Swirl fan diameter (mm)
ϕ	The viscous-dissipation function
ϕs	Parameter
ω	Specific dissipation rate (s^{-1})

SUPERSCRIPTS AND SUBSCRIPTS

b	Bulk
i	Inlet
m	Mean
s	Shell side
sr	Surface
t	Tube side
t,f	Tube with inserted swirl fan
t,s	Plain tube
w	Wall
eff	Effective property
i,j,k	Donates Cartesian coordinates direction takes the value of axis X,Y,Z

1. INTRODUCTION

Heat exchangers are found in the power generation field, and in numerous industrial applications. The shell and tube heat exchanger is the most versatile type of heat exchangers and is the one most widely used in these fields. That is due to their relatively simple construction and the multi-purpose application possibilities for gaseous and fluid media in a very large temperature and pressure range. This has led to increased levels of research experimentally, analytically and numerically on the heat transfer and hydraulic behavior of heat exchangers. [1]

Many factors enter into the design of heat exchangers, including thermal analysis, weight, size, pressure drop, and cost. Economics play a key role in the design and selection of heat exchanger equipment. The weight and size of heat exchangers are significant parameters in the overall application and thus may still be considered as variables involved in economic evaluation.

The calculation of convective heat transfer coefficients constitutes a crucial issue in designing and sizing any type of heat exchange device. Thus its correct determining permits for the proper selection of heat transfer area during designing of heat exchangers and calculation of the fluids outlet temperature. A lot of efforts have been made during experimental investigations of pressure drop and heat transfer in different types of heat exchangers to obtain proper heat transfer correlation formulas. [2]

The present study focused on thermal-hydraulic parameters investigations of shell and tube heat exchanger with and without inserted single fixed vane swirler per each tube in the tube side inlet. The aim of using vane swirler is as a heat transfer enhancement device for decreasing the weight and size to obtain the most possible cost reduction. The investigations are conducted for a wide range of vane swirler diameter, and blade angle in each tube. The effect of changing these parameters on heat transfer, friction factor, and the corresponding thermal enhancement factor are presented. The corresponding contours of temperature, pressure, velocity, and turbulence intensity, also flow path lines along the heat exchanger are presented. Effect of all these parameters on both heat transfer and friction factor are demonstrated. Finally, empirical correlations for Nusselt number and friction factor are developed, and compared with Kurtbus et al. [3] empirical correlation. Also, the corresponding relations between the heat transfer and friction factor are presented.

2. LITRATURE SURVEY

2.1 EXPERIMENTAL INVESTIGATIONS

The experiments primary concern on the determination of overall heat transfer coefficient and Nusselt number as a direct index on heat exchanger performance. Also, one of their concerns is to determine the pressure drop and friction factor at different geometric arrangements.

Kurtbas et al. [3] have investigated experimentally the effect of freely rotating propeller–type turbulators with variable angle (θ), diameter (D_b) and number of blades located in the inner pipe of a counter flow double pipe heat exchanger on heat transfer (Nu) of turbulent air flow at a Reynolds number range from 10^4 to 3×10^4, and developing the corresponding empirical correlations for Nusselt number as follows:

$$Nu = 0.343\,\mathrm{Re}^{0.62}(1+\tan\theta)^{-1.006} \times (D_b / D_p)^{0.625}(L_t / L_p)^{-0.336} \tag{1}$$

Where the correlation range is θ = 10º, 20º and 40º, D_b/D_p = 0.8, 0.83 and 0.87 and Re = 10,000 – 30,000.

The main conclusions from this investigation are as follows:

- Maximum decaying distance of swirl flow was found to be one third of pipe length.
- Lower blade angle, and minimum inter-turbulator distance (L_t/L_p) gives higher efficiency.
- Nusselt number increases with the decrease in blade angle and inter-turbulator distance, and with the increase in Reynolds number.
- Nusselt number with propeller type turbulators increases about 3.6 times that of plain pipe.

Eiamsa–ard et al. [4] have investigated experimentally the effect of regularly–spaced dual twisted tapes with variable twist and space ratios in comparison with single and dual full-length twisted tapes. The tapes located into a uniform wall heated pipe. Heat transfer and friction characteristics of turbulent air flow at a Reynolds number range from 4000 to 19000 are investigated. An empirical correlation for Nusselt number and friction factor of a plain tube case are developed as:

$$Nu = 0.017\,\mathrm{Re}^{0.82}\,\mathrm{Pr}^{0.4} \tag{2}$$

$$f = 3.1\,\mathrm{Re}^{-0.48} \tag{3}$$

Thianpong et al. [5] have investigated experimentally the effect of twisted tape with variable twist ratio, in a dimpled inner pipe of a counter flow double pipe heat exchanger with dimple variable pitch ratio. Heat transfer and friction characteristics of turbulent air flow at a Reynolds number range from 12000 to 44000 are investigated. An empirical correlation for Nusselt number and friction factor of the inner plain tube case are also given as:

$$Nu = 0.049\,\mathrm{Re}^{0.706}\,\mathrm{Pr}^{0.4} \tag{4}$$

$$f = 0.718\,\mathrm{Re}^{-0.309} \tag{5}$$

2.2 ANALYTICAL INVESTIGATIONS

In the present paper, it was found that the analytical methods with its corresponding empirical correlations of heat transfer and friction have limitations and are of doubtful accuracy.

For the tube side flow's friction correlations, Blasius [6] correlation for fully developed turbulent flow as follows.

$$f = 0.316\,\mathrm{Re}^{-0.25} \qquad \text{for } \mathrm{Re} \le 2 \times 10^4 \tag{6}$$

$$f = 0.184\,\mathrm{Re}^{-0.2} \qquad \text{for } \mathrm{Re} \ge 2 \times 10^4 \tag{7}$$

Petukhov correlation [7] for fully developed turbulent flow at $3000 \le \mathrm{Re} \le 5 \times 10^6$ is given as:

$$f \equiv (0.790\ln \mathrm{Re} - 1.64)^{-2} \tag{8}$$

For the tube side flow's heat transfer correlations, Colburn correlation [8] for fully developed (hydro-dynamically and thermally) turbulent flow in a smooth circular tube is given as:

$$Nu = 0.023\,\mathrm{Re}^{4/5}\,\mathrm{Pr}^{1/3} \tag{9}$$

The Dittus-Boelter equation [9] for fully developed turbulent flow is given as:

$$Nu = 0.023\,\mathrm{Re}^{4/5}\,\mathrm{Pr}^{na} \tag{10}$$

Where na = 0.4 for heating ($T_{sr} > T_m$) and 0.3 for cooling ($T_{sr} < T_m$), for the range of conditions (moderate temperature differences), $0.6 \le \mathrm{Pr} \le 160$, $\mathrm{Re} \ge 10{,}000$, $L/D \ge 10$

For the shell side flow, Bell-Delaware [10] method, the heat-transfer coefficient and pressure drop are estimated from correlations for flow over ideal tube-banks, and the effects of leakage, bypassing and flow in the window zone are allowed for by applying correction factors. Bell-Delaware method assumes that the flow rate and the thermo-physical properties of the shell-side fluid are specified; also shell-side geometrical parameters are known. This method considered as a very detailed method and is usually very accurate in estimating the shell side heat transfer coefficient and the pressure drop for common shell side geometric arrangements.

The correlation for shell-side heat transfer coefficient is [10]:

$$h_s = h_i(J_c J_l J_b J_s J_r) \tag{11}$$

Where,

h_s The shell side heat transfer coefficient

h_i The heat transfer coefficient for pure cross flow in ideal tube bank

J_c The segmental baffle window correction factor

J_l The baffle leakage correction factor

J_b The bypass correction factor, tube bundle to shell

J_s The unequal inlet/outlet baffle spacing correction factor, applicable only if such differences exist

J_r The laminar heat transfer correction factor, applicable for Re < 100

The correlation for shell-side pressure drop is [10]:

$$\Delta p_s = \Delta p_c + \Delta p_w + \Delta p_e \tag{12}$$

Where as shown in Fig. 1,

Δp_s The total shell-side pressure drop excluding nozzles

Δp_c The combined pressure drop of all the interior cross flow section (baffle tip to baffle tip)

Δp_w The combined pressure drop in all the windows crossed

Δp_e The pressure drop in the two end zones

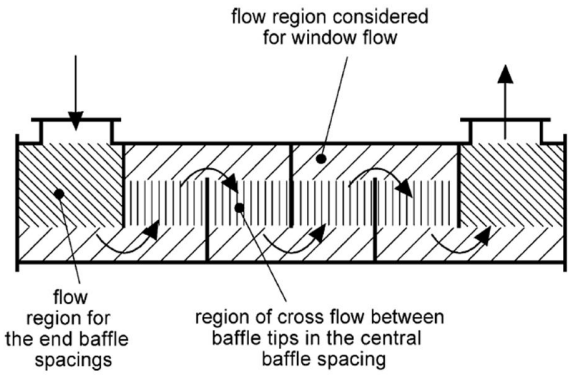

Fig. 1 The three components of the pressure drop (Δp_c, Δp_w, Δp_e) referred to the three flow zones. [11]

As a general conclusion, it can be said that correlation based approaches may indicate the existence of a weakness in design, but CFD simulations can also pin point the source and the location of the weakness. Using CFD, together with supporting experiments, may speed up the shell-and-tube heat exchanger design process and may improve the quality of the final design.

2.3 NUMERICAL INVESTIGATIONS

Ozden and Tari [12] have investigated numerically using the commercial CFD package FLUENT 6.3, the dependencies of the shell side geometrical parameters. The baffle spacing of 86, 62, 48, and 40 mm relative to number of baffles of 6, 8, 10, and 12, baffle cut ratio of 25% and 36% on the shell side heat transfer coefficient and the pressure drop at different shell side mass flow rate of 0.5, 1.0, and 2.0 kg/s.

The CFD simulations are performed for the shell side of a single tube pass shell and tube heat exchanger. Water is the shell side working fluid with inlet temperature of 300 K, and a constant tube wall temperature of 450 K.

The shell size inner diameter of 90 mm, length of 600 mm, tubes outer diameter of 20 mm, tube bundle geometry and pitch are triangular of 30 mm, number of tubes are 7 and the main conclusions from this investigation are as follows:

The $k-\varepsilon$ realizable turbulence model with first order discretization and the fine mesh of 1,360,000 elements is selected as the best simulation approach. For this heat exchanger geometry; 25% baffle cut gives slightly better results. Increasing the number of baffles would improve the heat transfer characteristics of the heat exchanger.

Also Ur-Rehman [13] has investigated using Fluent, the heat transfer coefficient and pressure drop of a un–baffled shell–and–tube heat exchanger and concluded that $k-\omega$ SST model, with low Reynolds correction, provides better results as compared to other models.

From the foregoing review, the three–dimensional numerical analysis for the thermal–hydraulic characteristics of the flow inside heat exchangers is still needed more modification and coordination. The most of previous work was focusing on experimental way and developing the corresponding correlations. This less of researches has motivated the present study. Numerical simulations of the turbulent, three-dimensional fluid flow and heat transfer were performed using ANSYS FLUENT and compared with the literature.

3. GOVERNING EQUATIONS AND TURBULENCE MODEL

Continuity Equation

$$\frac{\partial u}{\partial x}+\frac{\partial v}{\partial y}+\frac{\partial w}{\partial z}=0 \tag{13}$$

Momentum Equations

$$\rho\left(u\frac{\partial u}{\partial x}+v\frac{\partial u}{\partial y}+w\frac{\partial u}{\partial z}\right)=-\frac{\partial P}{\partial x}+\mu\left(\frac{\partial^2 u}{\partial x^2}+\frac{\partial^2 u}{\partial y^2}+\frac{\partial^2 u}{\partial z^2}\right) \quad \text{in the x-dir.} \tag{14}$$

$$\rho\left(u\frac{\partial v}{\partial x}+v\frac{\partial v}{\partial y}+w\frac{\partial v}{\partial z}\right)=-\frac{\partial P}{\partial y}+\mu\left(\frac{\partial^2 \upsilon}{\partial x^2}+\frac{\partial^2 \upsilon}{\partial y^2}+\frac{\partial^2 \upsilon}{\partial z^2}\right) \text{ in the y-dir.} \tag{15}$$

$$\rho\left(u\frac{\partial w}{\partial x}+v\frac{\partial w}{\partial y}+w\frac{\partial w}{\partial z}\right)=-\frac{\partial P}{\partial z}+\mu\left(\frac{\partial^2 w}{\partial x^2}+\frac{\partial^2 w}{\partial y^2}+\frac{\partial^2 w}{\partial z^2}\right) \text{ in the z-dir.} \tag{16}$$

Energy Equation

$$\rho c_v\left(u\frac{\partial T}{\partial x}+v\frac{\partial T}{\partial y}+w\frac{\partial T}{\partial z}\right)=\kappa\left(\frac{\partial^2 T}{\partial x^2}+\frac{\partial^2 T}{\partial y^2}+\frac{\partial^2 T}{\partial z^2}\right)+\phi \tag{17}$$

$$\phi=\mu\left[2\left(\frac{\partial u}{\partial x}\right)^2+2\left(\frac{\partial \upsilon}{\partial y}\right)^2+2\left(\frac{\partial w}{\partial z}\right)^2+\left(\frac{\partial \upsilon}{\partial x}+\frac{\partial u}{\partial y}\right)^2+\left(\frac{\partial w}{\partial y}+\frac{\partial v}{\partial z}\right)^2+\left(\frac{\partial u}{\partial z}+\frac{\partial w}{\partial x}\right)^2\right] \tag{18}$$

The RNG $k-\varepsilon$ Model

The RNG $k-\varepsilon$ model was derived using a rigorous statistical technique (called renormalization group theory). It is similar in form to the standard $k-\varepsilon$ model, but includes the following refinements:

- The RNG model has an additional term in its ε equation that significantly improves the accuracy for rapidly strained flows.
- The effect of swirl on turbulence is included in the RNG model which enhancing the accuracy for swirling flows.
- The RNG theory provides an analytical formula for turbulent Prandtl numbers, while the standard $k-\varepsilon$ model uses user-specified, constant values.
- While the standard $k-\varepsilon$ model is a high-Reynolds-number model, the RNG theory provides an analytically-derived differential formula for effective viscosity that accounts for low-Reynolds-number effects. Effective use of this feature does, however, depend on an appropriate treatment of the near-wall region.

These features make the RNG $k-\varepsilon$ model more accurate and reliable for a wider class of flows than the standard $k-\varepsilon$ model. [14]

The transport equations for the turbulence kinetic energy k and its dissipation rate ε are:

$$\rho\frac{\partial k}{\partial t}+\rho U_i\frac{\partial k}{\partial x_i}=\frac{\partial}{\partial x_j}\left[\alpha_k\mu_{eff}\frac{\partial k}{\partial x_j}\right]+G_k+G_b-\rho\varepsilon-Y_M+S_K \tag{15}$$

$$\rho\frac{\partial \varepsilon}{\partial t}+\rho U_j\frac{\partial \varepsilon}{\partial x_j}=\frac{\partial}{\partial x_j}\left[\alpha_\varepsilon\mu_{eff}\frac{\partial \varepsilon}{\partial x_j}\right]+C_{1\varepsilon}\frac{\varepsilon}{k}(G_k+C_{3\varepsilon}G_b)-C_{2\varepsilon}\rho\frac{\varepsilon^2}{k}-R_\varepsilon+S_\varepsilon \tag{16}$$

4. MODEL CONFIGURATION

The shell and tube heat exchanger model geometry presented in Fig. 2(a) was made exactly as Ozden and Tari [12], were model main geometrical parameters are presented in Table 1. The effect of baffle clearance, and tube to baffle bypass leakages are neglected.

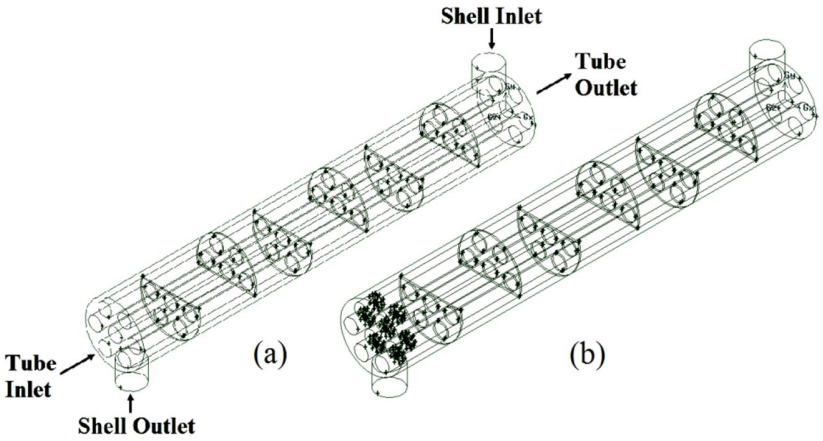

Fig. 2 Model configuration for (a) plain tube case, and (b) single inserted vane swirler per each tube.

Table 1 Heat exchanger dimensions

Description	Unit	Value
Shell diameter	mm	90
Shell inlet nozzle diameter	mm	36
Tube diameter	mm	20
Heat exchanger length	mm	600
No. of tube	--	7
Tube arrangement	--	Triangular 30º
No. of baffles	--	6
Baffle cut ratio	%	36

The inserted single vane swirler per each tube is of eight blades as in Fig. 3, while vane swirler diameter and blade angle are varied as in Table 2. Vane swirler location in each tube at distance of 20 mm from tube side inlet to eliminate the entrance effect as shown in Fig. 2(b).

Table 2 Vane swirler geometry.

Vane swirler diameter (φ)	5 mm		10 mm	15 mm		18 mm	19 mm
Vane swirler angle (θ)	15º	20º	30º	35º	40º	45º	60º

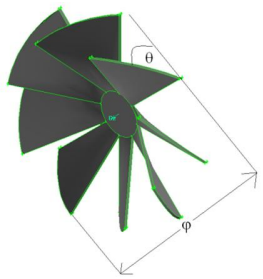

Fig. 3 Eight blades vane swirler geometry.

5. MODEL BOUNDARY CONDITIONS

Present study accomplished in two parts, the main part is the shell and tube modeling, and the other part is the shell side modelling, which are used only for shell side validation with Ozden and Tari [12]. Detailed boundary conditions for both parts are as seen in Table 3.

Table 3 Model boundary conditions.

	Description	Symbol	Unit	Shell and tube modeling	Shell side modeling
Shell side	Working fluid	--	--	Water	Water
	Inlet mass flow rate	$\dot{m}_s$	kg/s	0.5	0.5
				1.0	1.0
				2.0	2.0
	Inlet Reynolds number	Re_s	--	10290	10290
				20370	20370
				40740	40740
	inlet temperature	$T_{s,i}$	K	350	300
Tube side	Working fluid	--	--	Water	--
	Total inlet mass flow rate	$\dot{m}_t$	kg/s	0.5	--
				1.0	--
				2.0	--
	Inlet Reynolds number	Re_t	--	5318	--
				10637	--
				21274	--
	inlet temperature	$T_{t,i}$	K	300	--
	Wall temperature	$T_{t,w}$	K	--	450

6. MODEL SOLVER PARAMETERS

- Piecewise-linear profile for themo-physical properties between inlet hot and cold fluids.
- Shell and tube sides' velocity-inlet type.
- Shell and tube sides' pressure-outlet type.
- RNG $k-\varepsilon$ turbulence model with non-equilibrium near-wall treatment functions as been verified in an earlier investigation [15].
- Under-Relaxation factors as FLUENT default except energy and turbulent viscosity of 0.8.
- Pressure-Velocity coupling is SIMPLE.
- 2nd order upwind discretization schemes as will be verified later on in this chapter.

7. HEAT TRANSFER AND FRICTION CALCULATIONS

The main dimensionless parameter representing heat transfer is the Nusselt number which can be calculated as stated in Ref. [16] and it can be written as,

$$Nu = \frac{hD}{\kappa} \tag{17}$$

Where,

h: is the heat transfer coefficient (W/m^2.K) calculated for the shell side from Equ. 11 as detailed in Ref. [10] and using the ANSYS FLUENT model resultant temperatures and pressures, and for the tube side the following equation is applied,

$$h_t = \frac{\dot{m}_t c_{p,t} \Delta T_t}{A_{t,sur}(T_{t,w,av} - T_b)} \tag{18}$$

Where,
D: is the tube diameter (m) for tube side calculation and is the equivalent hydraulic diameter for the shell side calculation as detailed in Ref. [10].
κ: is the thermal conductivity (W/m.K) calculated at the bulk temperature.
$\dot{m}_t$: is the tube side mass flow rate (kg/s).
$c_{p,t}$: is the pressure coefficient (J/kg.K) calculated at the bulk temperature.
$A_{t,sur}$: is the tube internal surface area (m^2).
$T_{t,w,av}$: is the tube side average wall temperature obtained from ANSYS FLUENT model.
T_b: is the bulk temperature (K) which is the mathematical average temperature between inlet and outlet.

The main dimensionless parameter representing friction is the friction factor which can be calculated as stated in Ref. [16] and it can be written as,

$$f = \frac{\Delta p}{\frac{L}{D}\frac{\rho u^2}{2}} \tag{19}$$

Where,
Δp: is the pressure drop between inlet and outlet obtained from ANSYS FLUENT model.
L: is the tube or shell length (m).
ρ: is the density (kg/m^3) calculated at the bulk temperature.
u: is the inlet velocity (m/s).

The main dimensionless parameter representing the relation between heat transfer and friction in the tube side, and the resultant enhancement in heat transfer with respect to friction loss; is the thermal enhancement factor which can be calculated as stated in Ref. [17] and it can be written as follows:

$$TEF = \frac{(\mathrm{Nu}_t / Nu_p)}{(f_t / f_p)^{1/3}} \tag{20}$$

Where the subscripts; t referred to tubes with inserted vane swirlers case and p referred to plain tubes case.

8. HEAT EXCHANGER GRID INDEPENDENCY CHECK

Different mesh sizes have been used of 4,089,747, 2,132,064, 1,767,675, and 1,534,864 cells. The mesh size of 2,132,064 cells are found to be the most suitable mesh size for the present study model as have been verified in an earlier investigation [15].

9. TURBULENCE MODELS VALIDATION

Different models have been used in an earlier investigation [15] which are standard $k-\varepsilon$, RNG $k-\varepsilon$, Realizable $k-\varepsilon$, $k-\omega$ SST, and RSM. The 2nd order RNG $k-\varepsilon$ model with non-equilibrium wall function and 2nd order pressure discretization scheme show the best results compared to literature.

10. TUBE SIDE VALIDATION

Shell and tube modeling as presented in Table 3 are used for the tube side validation of the shell and tube heat exchanger in comparison with the following correlations:

Thianpong et al. [5] presented an empirical correlation developed from the experimental results, where these experimental results are showing a maximum uncertainty in results of ± 10% for Nusselt number and ± 15% for friction factor, also a deviation of ± 7% for Nusselt number results in comparison with Dittus-Boelter [9] correlation and ± 18% for friction factor results in comparison with Blasius [6] correlation.

Eiamsa-ard et al. [4] empirical correlations developed from the experimental results, where these correlations showing a maximum deviation of 6.7% for Nusselt number results in comparison with Colburn [8] correlation, and a maximum deviation of 33.8% for friction factor results in comparison with Petukhov [7] correlation.

The present tube side predictions in comparison with the empirical correlations of Thianpong et al. [5], Eiamsa-ard et al. [4], Colburn [8] and Petukhov [7] at mass flow rate of 0.5, 1.0, and 2.0 kg/s, and the corresponding Reynolds numbers are 5319, 10637, and 21274 respectively are presented in Figs. 4 and 5.

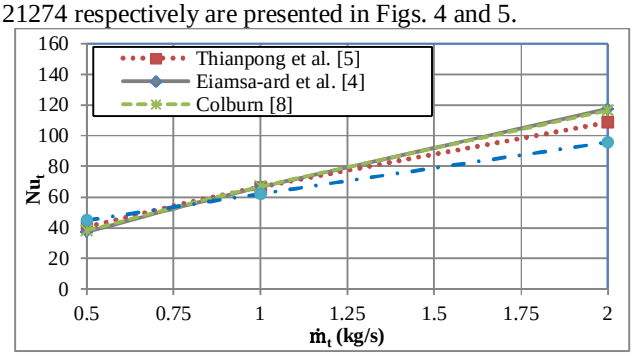

Fig. 4 Present tube side Nusselt number in comparison with Thianpong et al. [5], Eiamsa-ard et al. [4], and Colburn [8] correlations.

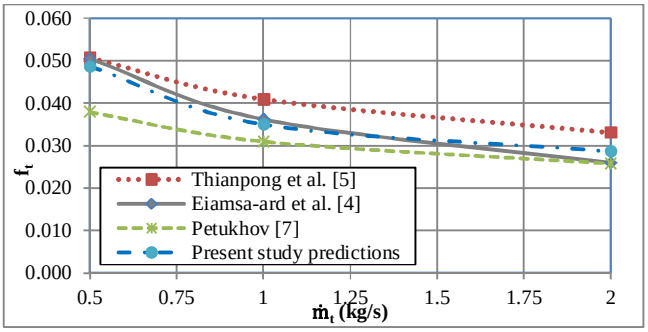

Fig. 5 Present tube side friction factor in comparison with Thianpong et al. [5], Eiamsa-ard et al. [4], and Petukhov [7] correlations.

The present study predictions for tube side of shell and tube heat exchanger in comparison with the empirical correlations of Thianpong et al. [5], Eiamsa-ard et al. [4], Colburn [8] and Petukhov [7] is presented in Figs. 4 and 5, showing a maximum deviation of 11.9%, 19.7% and 17.8% for Nusselt number predictions in comparison with the correlations of Thianpong, et al. [5], Eiamsa-ard et al. [4], and Colburn [8] respectively, while a maximum deviation of 14.5%, 10.4% and 28.6% for friction factor predictions in comparison with the correlations of Thianpong et al. [5], Eiamsa-ard et al. [4], and Colburn [8] respectively. The results of the present study predictions reasonably agree well with the presented correlations as it's laying between them although the deviation in Nusselt number is found increasing at high mass flow rates, which may occur due to that the outer wall of tubes in the heat exchanger are exposed to a complicated heat transfer pattern that the simple cases used in these correlations for constant heat flux or constant wall temperature.

11. SHELL SIDE VALIDATION

Shell side modelling as presented in Table 3 are used for the shell side validation of the shell and tube heat exchanger with Ozden and Tari [12] predictions and Bell-Delaware [10] correlation.

Ozden and Tari [12] predictions are showing a maximum deviation of 34.7% for heat transfer coefficient predictions in comparison with that of Bell-Delaware [10] correlation, and a maximum deviation of 34.2% for pressure drop predictions in comparison with that of Bell-Delaware [10] correlation.

The present study predictions for shell side of the shell and tube heat exchanger in comparison with Ozden and Tari [12] predictions and Bell-Delaware [10] correlation are presented in Figs. 6 and 7.

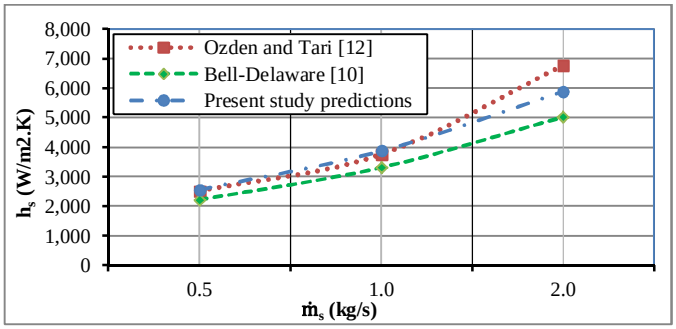

Fig. 6 Present shell side heat transfer coefficient in comparison with Ozden and Tari [12] and Bell-Delaware [10].

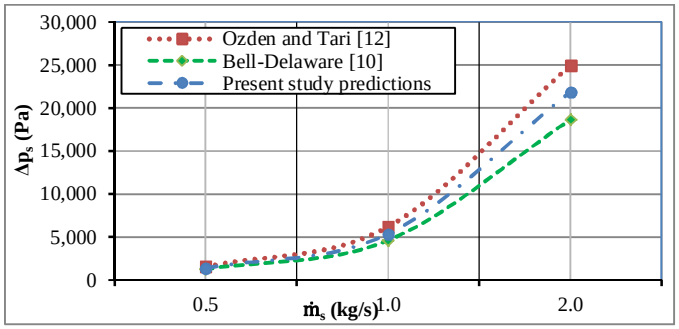

Fig. 7 Present Shell side pressure drop in comparison with Ozden and Tari [12] and Bell-Delaware [10].

The results presented in Figs. 6 and 7 showing a maximum deviation of 14.1% and 15.8% for heat transfer coefficient predictions in comparison with Ozden and Tari [12] predictions and Bell-Delaware [10] correlation, respectively. While a maximum deviation of 20% and 8.1% for pressure drop predictions in comparison with Ozden and Tari [12] predictions and Bell-Delaware [10] correlation.

Consequently, the results of the present study predictions reasonably agree well with literature predictions and correlations as it is laying between them although the deviation is increasing at high mass flow rates, which may occur due to that Ozden and Tari [12] used a different turbulence model (Realizable $k-\varepsilon$ model), different discretization scheme (1st order upwind), and different mesh size of 1,360,000 elements.

12. RESULTS AND DISCUSSIONS

12.1 FLOW BEHAVIOUR FOR SINGLE VANE SWIRLER PER EACH TUBE

Flow and heat transfer have interaction on each other in convective heat transfer processes, therefore, thermal augmentation has a relationship to the distributions of both velocity and temperature fields. To explain the effect of vane swirlers insertion on the heat transfer and flow resistance, different contours and path lines plots will be presented. The plots of temperature contours, pressure contours, velocity contours, turbulence intensity contours, and flow path lines along the heat exchanger of plain tubes and tubes with inserted vane swirlers of φ = 19 mm and θ = 15° at 20 mm from tubes inlet, at the case of $\dot{m}$ = 2 kg/s are presented for this purpose.
The presented contour plots are taken at four different positions, a cross section along tube length in-line with three cross section side views at locations of 26 mm, 300 mm, and 574 mm from tubes inlet. These positions are relative to the positions at the middle of shell side outlet nozzle, the middle of the heat exchanger, and the middle of shell side inlet nozzle, respectively.

12.1.1 TEMPERATURE CONTOURS

The temperature contours in Fig. 8.1(a) for the plain tubes case show that the thermal boundary layer grows thicker. In other words, temperature gradient near the wall becomes smaller. While, for the inserted vane swirlers case, as in Fig. 8.1(b), it is observed that there is a major change in temperature gradient indicating the better fluid mixing from using vane swirlers where higher turbulence intensity is induced. Going along tubes length, the near-wall swirls will be weakened, and thus leading to a weakening in the heat transfer.
Higher temperature gradient in the tube side indicates a larger heat flux between tube walls, and fluid resulting in large local heat transfer, and hence global heat transfer. This is reflected in the Nusselt number (hence the heat transfer coefficient), which is larger for inserted vane swirlers than for plain tubes. Consequently it can be concluded that for a fixed Reynolds number the heat transfer enhancement increased by inserting vane swirlers in the tubes of heat exchangers. In contrast, for a fixed inlet velocity the heat transfer can be improved by the inserted vane swirlers.

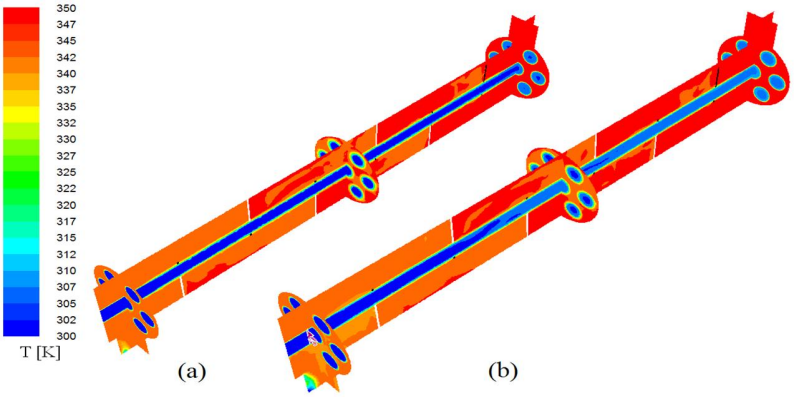

Fig. 8 Temperature contours for (a) plain tubes, and (b) single vane swirler.

12.1.2 PRESSURE CONTOURS

The pressure drop for the vane swirlers inserts as in Fig. 9 (b) is much higher than that for the plain tube case as in Fig. 9 (a), due to the flow blockage (body resistance) in the area of vane swirlers. Thus it is an essential issue when investigating heat exchanger with inserted flow enhancer, the heat transfer and pressure drop should be considered at a balance for design and operation.

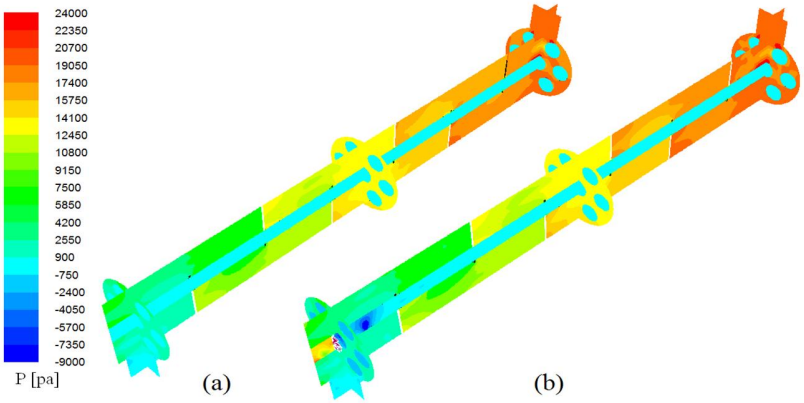

Fig. 9 Pressure contours for (a) plain tubes, and (b) single vane swirler.

12.1.3 VELOCITY CONTOURS

For the plain tube case as in Fig. 10 (a) the high-speed flow region appears in the central part of the tube away from walls and no such a near-wall swirls. Correspondingly, the thermal boundary layer grows thicker, i.e., the heat transfer at the wall will be very low. While, for tubes with inserted vane swirlers as in Fig. 10 (b), the velocity near the wall is much higher, which means a much stronger disturbance and fluid mixing of the boundary layer and higher heat transfer. Going further in tubes weakens the swirls till the near-wall swirls disappeared in the whole cross section area.

As a result from the presented temperature, pressure, and velocity contours; the vane swirlers insertion decreases the flow passage area, resulting in higher velocity and temperature gradient in the tube side, hence the higher pressure drop and heat transfer.

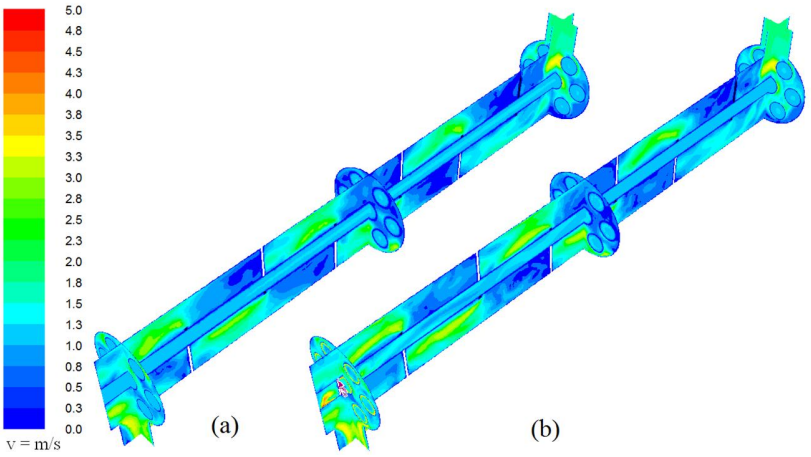

Fig. 10 Velocity contours for (a) plain tubes, and (b) single vane swirler.

12.1.4 TURBULENCE INTENSITY CONTOURS

From Fig. 11, the insertion of vane swirlers, turbulence intensity contours exhibit obvious variations in the area near vane swirlers as compared with same area of plain tubes. Hence, the tube with inserted vane swirlers is more contributively than the plain tube to the benefit of heat transfer enhancement with the promoted flow turbulence resulting in higher heat transfer rate than that of plain tubes. Furthermore the turbulence intensity decreases, this is because the flow swirls decrease as distance increases from the vane swirlers, and the axisymmetric swirl streams impinged to the tube wall become less and less, which indicates that the heat transfer deteriorates.

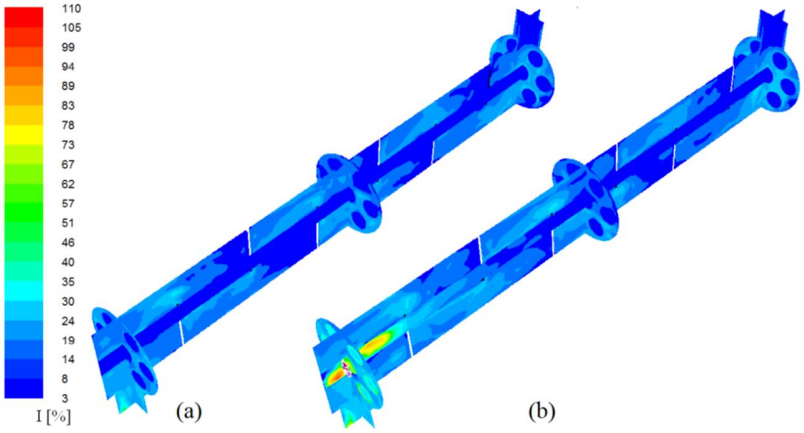

Fig. 11 Turbulence intensity contours for (a) plain tubes, and (b) single vane swirler.

12.1.5 FLOW PATH LINES

Flow path lines in the heat exchanger without and with inserted vane swirlers in the tube side are depicted in Figs. 12 – 16 with different colors for different path lines. Figure 12 presents the local distributions of the path lines for the heat exchanger cross section along heat exchanger between tubes and shell sides. Various cross section planes locations for the following Figs. 13 – 16 are also presented. For a clear presentation of flow path lines only the middle tube of the tube side is presented.

For shell side flow, the main stream in the shell side passing the cut window of the 1st baffle plate hits the next baffle plate, and the direction of the flow is changed. Unwanted recirculation zones appear in the corner of the baffle leading to deteriorate the convective

heat transfer. Depends on both the baffle cut and the baffle spacing values optimization the cross flow paths are established throughout the shell volume and the recirculation zones disappear. Effects of these values are studied in Ref. [12], so it will not be considered in the present study.

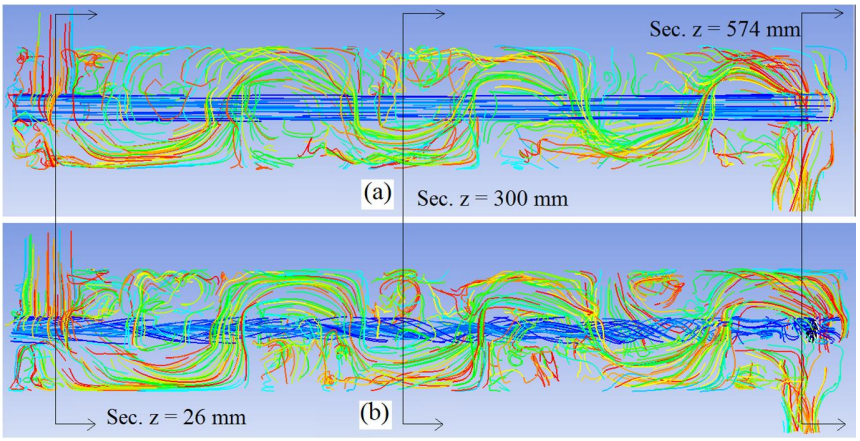

Fig. 12 Path lines on cross section plane for (a) plain tubes, and (b) single vane swirler.

For tube side flow, Figs. 13 (a) and 13 (b) represents the path line of the fluid flow through the tube side inlet without and with inserted vane swirlers respectively. It can be observed that for plain tubes flow type is straight flow. While for tubes with inserted vane swirlers; the flow behind the vane swirlers is separated after passing the eight blades of vane swirlers inducing a swirl flows along tubes pipe length. This flow pattern can help to increase better flow mixing, the heat transfer and turbulence intensity between the tubes walls and the core flows.

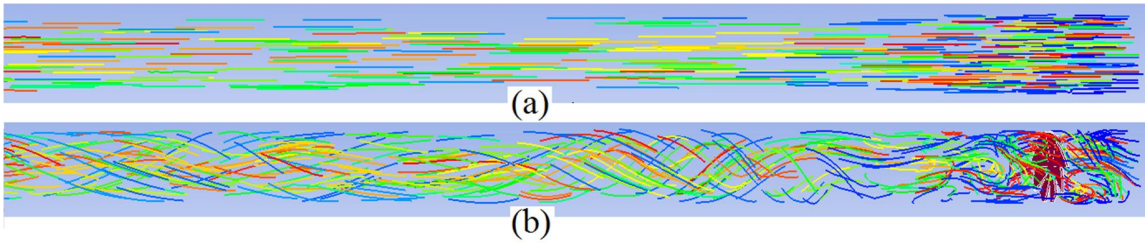

Fig. 13 Path lines at tube side inlet for (a) plain tubes, and (b) single vane swirler.

Figure 14 presents the local distributions of the flow path lines for the tube and shell sides, for heat exchanger cross section plane at z = 26 mm from tube side inlet, relative to the position at the middle of shell side outlet nozzle. Path lines plot in Fig. 14 (b) show the flow swirling at inlet region around inserted vane swirlers in the tube side. This region is a major reason of pressure drop due to impingement on vane swirlers blades. While, Fig. 14 (a) show the straight flow type in the tube side for plain tubes case.

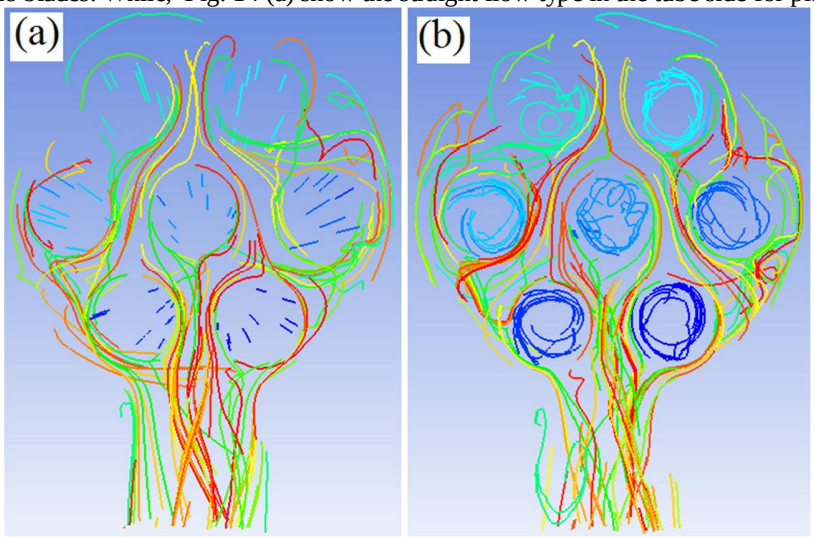

Fig. 14 Path lines on cross section plane z = 26 mm for (a) plain tubes, and (b) single vane swirler.

Figure 15 presents the local distributions of the flow path lines for the tube and shell sides, for heat exchanger cross section plane at z = 300 mm from tube side inlet, relative to the position at the middle of the heat exchanger. Path lines plot in Fig. 15 (b) show the continues flow swirling caused by the inserted vane swirlers but with less intensity from decaying effect far away from vane swirlers. While, Fig. 15 (a) show that still the flow is straight in the tube side for plain tubes case.

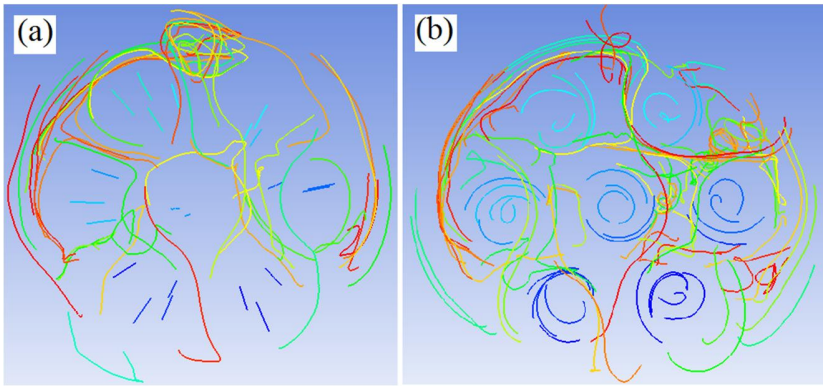

Fig. 15 Path lines on cross section plane z = 300 mm for (a) plain tubes, and (b) single vane swirler.

Figure 16 presents the local distributions of the flow path lines for the tube and shell sides, for heat exchanger cross section plane at z = 574 mm from tube side inlet, relative to the position at the middle of shell side inlet nozzle. Path lines plot in Fig. 16 (b) show continues flow swirling caused by the inserted vane swirlers but with less intensity than in section z = 300 mm as the decaying is much affecting on the flow path lines. While, Fig. 16 (a) show that still the flow is straight in the tube side for plain tubes case.

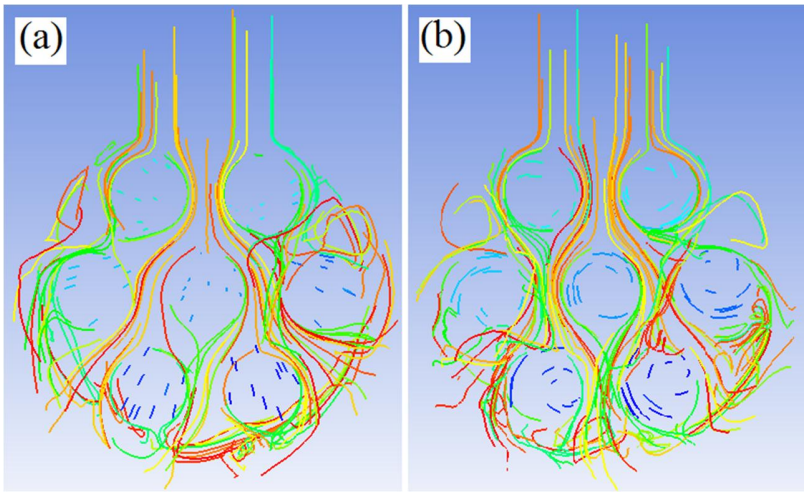

Fig. 16 Path lines on cross section plane z = 574 mm for (a) plain tubes, and (b) single vane swirler.

12.2 HEAT TRANSFER FOR SINGLE VANE SWIRLER PER EACH TUBE

In case of fixed vane swirler diameter, the influence of using the inserted fixed vane swirlers in the inlet of the tube side with different blade angles (θ = 15º, 20º, 30º, 35º,40º, 45º and 60º) on heat transfer for fixed vane swirlers diameter of (φ = 5 mm, 10 mm, 15 mm and 19 mm) as follows:

For φ = 5 mm as shown in the following Fig. 17 which shows that no noticeable increase with the insertion of the 5 mm vane swirlers at different blade angles than that in the case of plain tubes which couldn't be used as flow enhancement device.

For φ = 10 mm as shown in the following Fig. 18 which shows that a small increase in heat transfer than that of plain tube with the decrease in blade angle at higher mass flow rates and the effect decreased with the increase in blade angle which reaches a maximum of about 5% enhancement in heat transfer at θ = 15º.

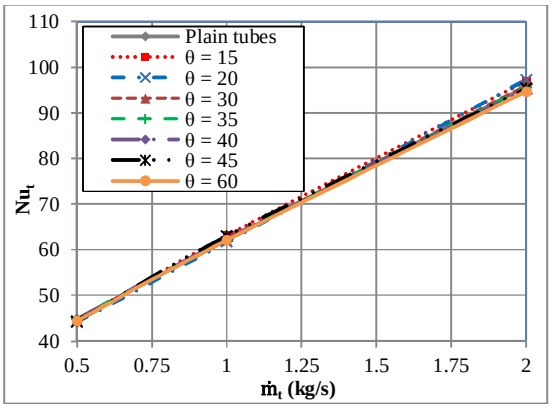

Fig. 17 Tube side Nusselt number vs. mass flow rate for φ = 5 mm.

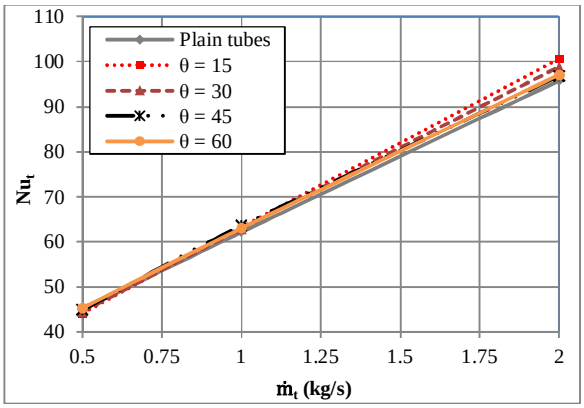

Fig. 18 Tube side Nusselt number vs. mass flow rate for φ = 10 mm.

For both φ = 15 mm and 19 mm as shown in the following Figs. 19 – 22 an obvious enhancement in heat transfer can be found which increases with the decrease in blade angle and increase in mass flow rate which reaches a maximum enhancement in heat transfer than that of plain tube at θ = 15° of 19% for φ = 15 mm and 62% for φ = 19 mm as shown in the following Figs. 21 and 22 for tube side Nusselt number ratio (Nu_t/Nu_p) for values of tube side Nusselt number with inserted vane swirlers divided by values of tube side Nusselt number of plain tubes case, which means that smaller blade angle generates more efficient flow blockage giving stronger turbulence intensity and thus superior heat transfer rate but this should be considered in the light of the corresponding friction to assure the superity of the system.

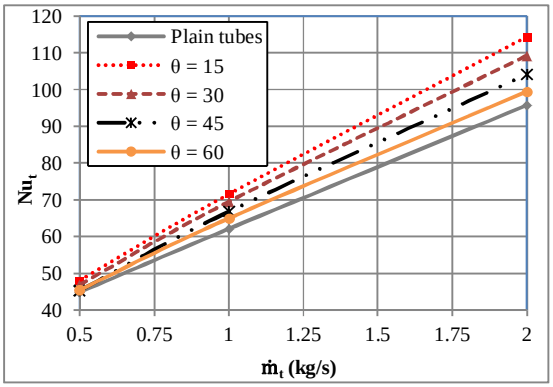

Fig. 19 Tube side Nusselt number vs. mass flow rate for φ = 15 mm.

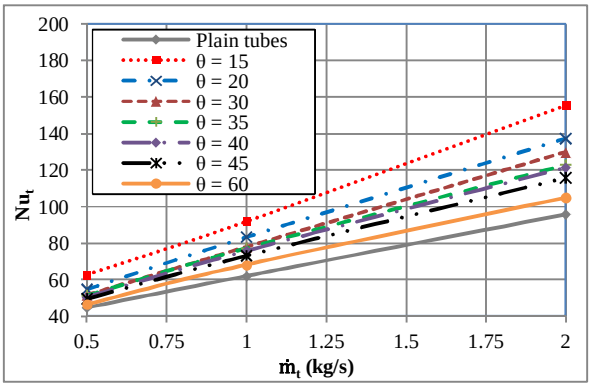

Fig. 20 Tube side Nusselt number vs. mass flow rate for φ = 19 mm.

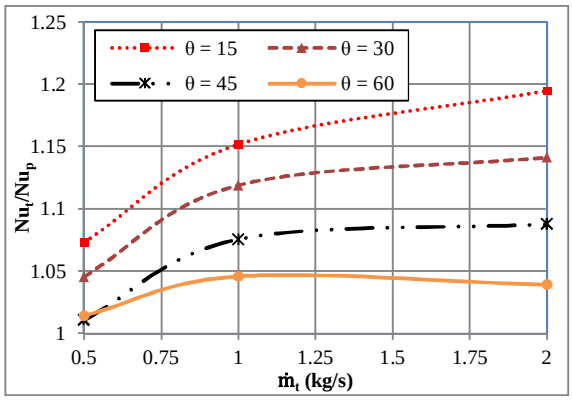

Fig. 21 Tube side Nusselt number ratio vs. mass flow rate for φ = 15 mm.

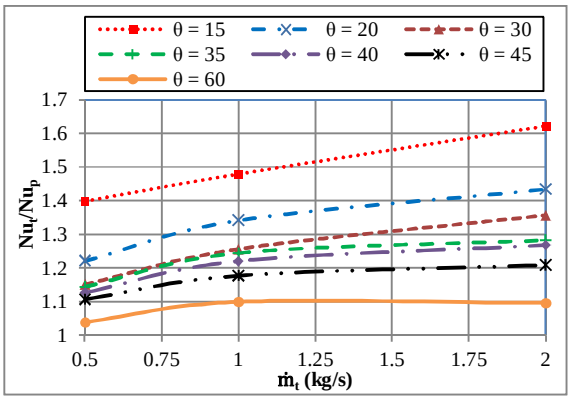

Fig. 22 Tube side Nusselt number ratio vs. mass flow rate for φ = 19 mm.

The shell side heat transfer doesn't noticeably affected by the insertion of the flow enhancer as the Nusselt number range of shell side is about ten times that of tube side which lead us to the great need to enhance the tube side heat transfer to increase the efficiency of

the system which reduces in the same time heat exchanger size and cost. Figure 23 for shell side Nusselt number at φ = 19 mm given as a demonstration to the said effect.

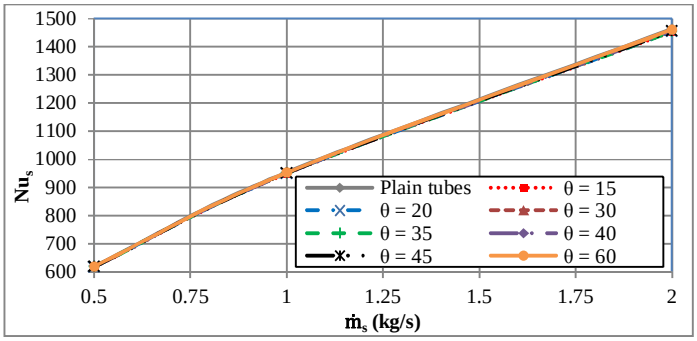

Fig. 23 Shell side Nusselt number vs. mass flow rate for φ = 19 mm.

In case of fixed blade angle, the influence of using the inserted fixed vane swirlers in the inlet of the tube side with different vane swirlers diameter (φ = 5 mm, 10 mm, 15 mm and 19 mm) on heat transfer for fixed blade angle of (θ = 15º, 30º, 45º and 60º) as follows:

For θ = 15º as shown in the following Figs. 24 and 25 the enhancement in heat transfer increases significantly with the increase in vane swirlers diameter and the increase ratio increases with the increase in mass flow rate and the enhancement reaches its maximum value of 62% at φ = 19 mm, which means that higher vane swirlers diameter generates more efficient flow blockage giving stronger turbulence intensity and thus superior heat transfer rate but also should be considered in the light of the corresponding friction to assure the superity of the system.

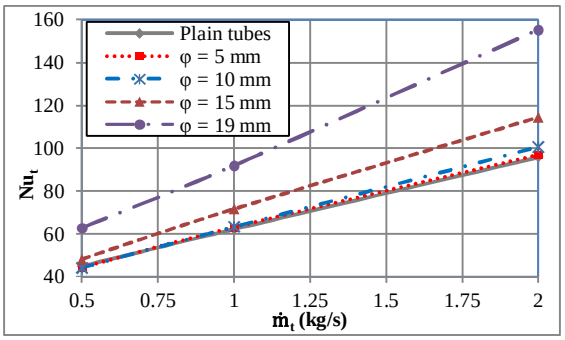

Fig. 24 Tube side Nusselt number vs. mass flow rate for θ = 15º.

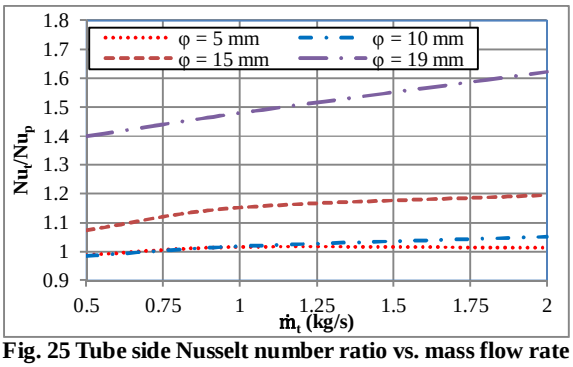

Fig. 25 Tube side Nusselt number ratio vs. mass flow rate for θ = 15º.

For θ = 30º as shown in the following Figs. 26 and 27 the enhancement in heat transfer increases gradually with the increase in vane swirlers diameter and the increase ratio increases with the increase in mass flow rate and the enhancement reaches its maximum value of 36% at φ = 19 mm, which assure as previously mentioned in the above paragraph for the benefits of flow blockage.

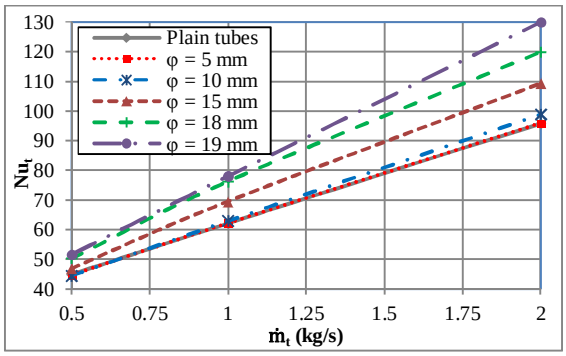

Fig. 26 Tube side Nusselt number vs. mass flow rate for θ = 30º.

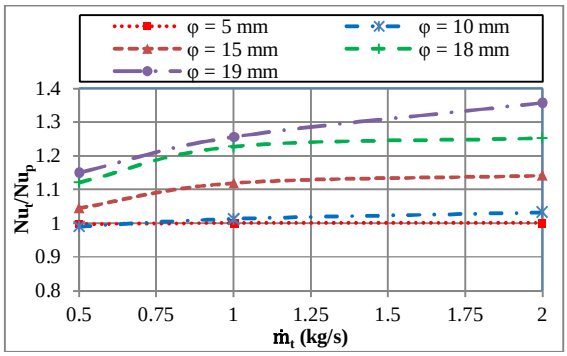

Fig. 27 Tube side Nusselt number ratio vs. mass flow rate for θ = 30º.

For θ = 45º as shown in the following Figs. 28 and 29 the enhancement in heat transfer is almost negligible for φ = 5 mm and 10 mm and then increases with the increase in vane swirlers diameter at φ = 15 mm and 19 mm and the increase ratio increases with the increase in mass flow rate and the enhancement reaches its maximum value of 21% at φ = 19, which shows that with the increase in blade angle the flow blockage decreases and consequently its effect on heat transfer enhancement even though the vane swirlers diameter increases.

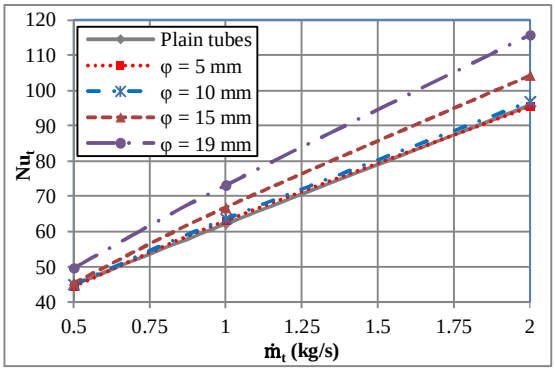

Fig. 28 Tube side Nusselt number vs. mass flow rate for θ = 45º.

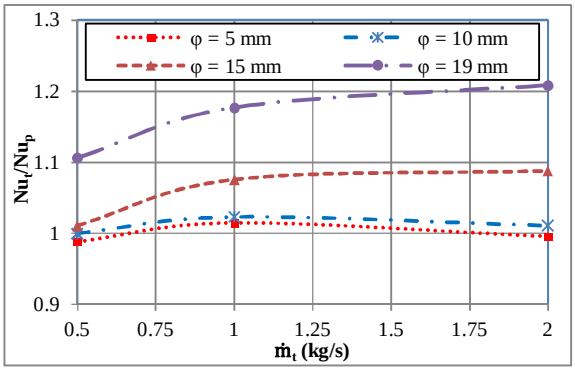

Fig. 29 Tube side Nusselt number ratio vs. mass flow rate for θ = 45º.

For θ = 60º as shown in the following Figs. 30 and 31 the enhancement in heat transfer is almost negligible for φ = 5 mm and 10 mm and then increases with the increase in vane swirlers diameter at φ = 15 mm and 19 mm and the increase ratio increases with the increase in mass flow rate and the enhancement reaches its maximum value of 10% at φ = 19, which shows that with a more increase in blade angle the flow blockage decreases significantly and consequently its effect on heat transfer enhancement even though the vane swirlers diameter increases.

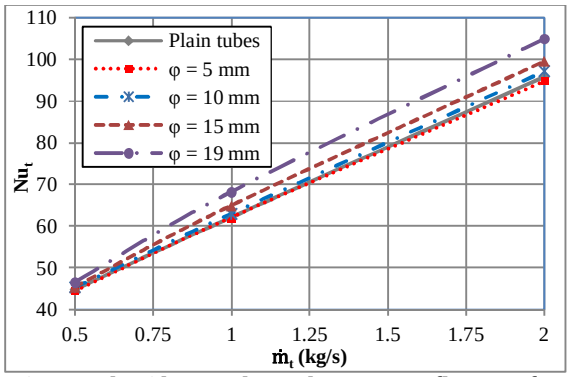

Fig. 30 Tube side Nusselt number vs. mass flow rate for θ = 60º.

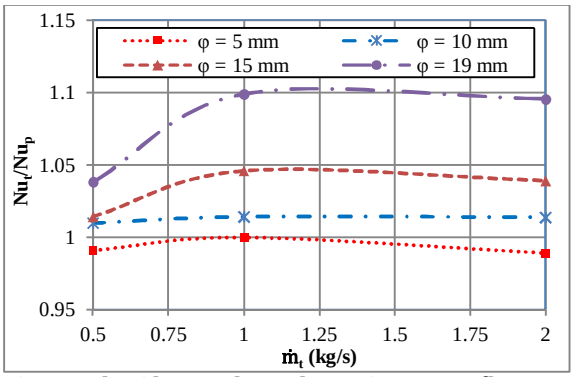

Fig. 31 Tube side Nusselt number ratio vs. mass flow rate for θ = 60º.

12.3 FRICTION FACTOR FOR SINGLE VANE SWIRLER PER EACH TUBE

In case of fixed vane swirler diameter, The influence of using the inserted fixed vane swirlers in the inlet of the tube side with different blade angles (θ = 15º, 20º, 30º, 35º, 40º, 45º and 60º) on friction factor for fixed vane swirlers diameter of (φ = 5 mm, 10 mm, 15 mm and 19 mm) as follows:

For φ = 5 mm influence of inserted vane swirlers with different blade angles on the friction factor is presented in Fig. 32 show that the friction factor decreases with increasing mass flow rate. Also the values of friction factor for different blade angle are higher than those of plain tubes although as previously shown that no noticeable increase in heat transfer values than those of plain tubes which again assure that no benefits can be taken from using 5 mm vane swirlers and only higher levels of friction factor.

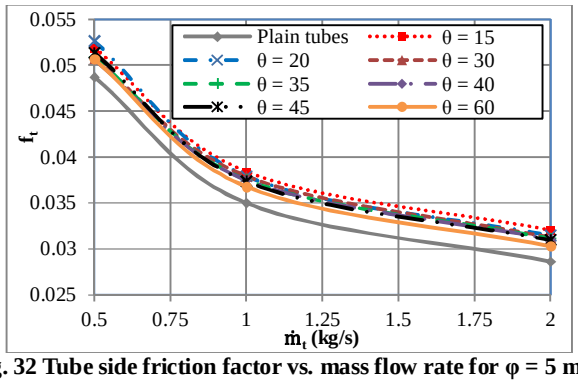

Fig. 32 Tube side friction factor vs. mass flow rate for φ = 5 mm.

For φ = 10 mm influence of inserted vane swirlers with different blade angles on the friction factor and friction factor ratio is presented in Figs. 33 and 34 show the same behaviour as disused in the last paragraph of friction factor with different blade angles and increase in mass flow rate but for this case a higher level of friction factor is found than those of plain tubes due to a greater flow interruption and thus inertial forces in the boundary layer becomes with the increase in vane swirler diameter and the friction factor increase cause by the inserted vane swirlers with blade angles, θ = 15º, 30º, 45º and 60º are respectively found to be maximum of 62%, 49%, 37% and 23% greater than those of plain tubes, which considerably very low relative to bigger vane swirlers diameter.

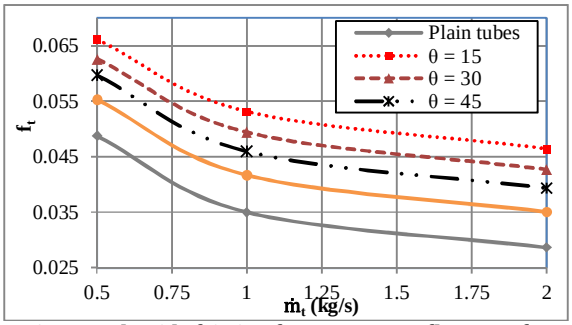

Fig. 33 Tube side friction factor vs. mass flow rate for φ = 10 mm.

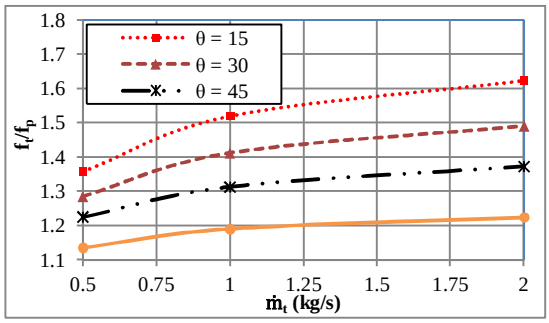

Fig. 34 Tube side friction factor ratio vs. mass flow rate for φ = 10 mm.

For both φ = 15 mm and 19 mm influence of inserted vane swirlers with different blade angles on the friction factor and friction factor ratio is presented in Figs. 35 to 38, and again the friction factor decreases with increasing mass flow rate. It is also visible that the use of these two big vane swirlers diameters relative to 20 mm tube diameter leads to a substantial increase in friction factor over that in the plain tube. One can observe from the figures that at the given mass flow rate, friction factor increase with the decrease in the blade angle. Since at a smaller blade angle, a double effect are found, higher levels of flow blockage due to the big vane swirlers diameter and a greater flow interruption and thus inertial forces in the boundary layer becomes. The friction factor increases cause by the inserted vane swirlers with the blade angle, 15º, 30º, 45º and 60º for φ = 15 mm are respectively found to be a maximum of 6.1, 4.0, 2.5 and 1.75 times of those in the plain tube and with the blade angle, 15º, 20º, 30º, 35º, 40º, 45º and 60º for φ = 19 mm are respectively found to be a maximum of 58.8, 28.9, 12.3, 9.3, 6.7, 5 and 2.5 times of those in the plain tube, which one can concluded a huge increase in friction with decrease in blade angle in these two vane swirlers diameter. In addition, the friction factor ratio noticeably increases with increasing mass flow rate for the entire range determined.

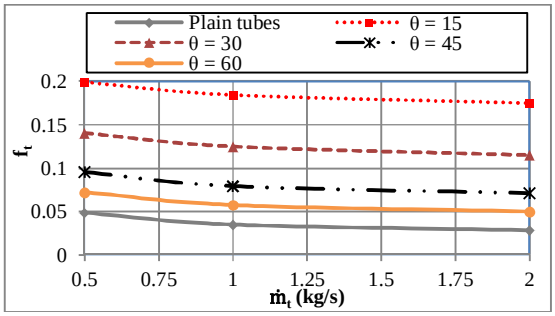

Fig. 35 Tube side friction factor vs. mass flow rate for φ = 15 mm.

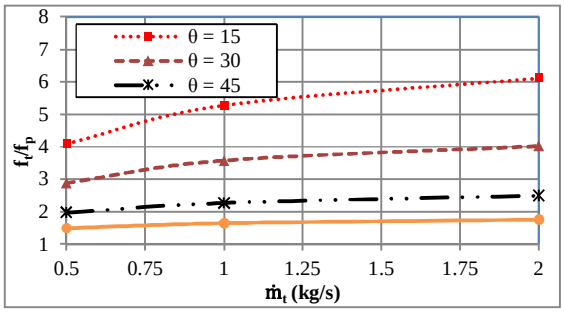

Fig. 36 Tube side friction factor ratio vs. mass flow rate for φ = 15 mm.

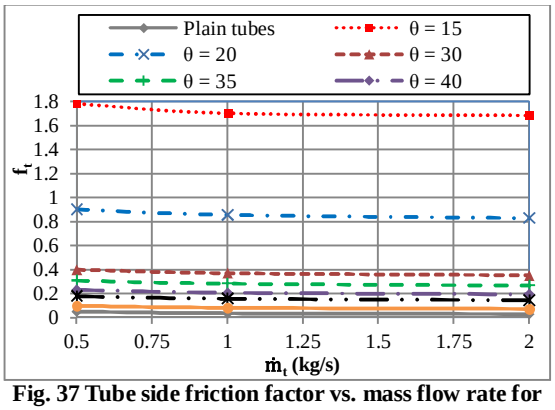

Fig. 37 Tube side friction factor vs. mass flow rate for φ = 19 mm.

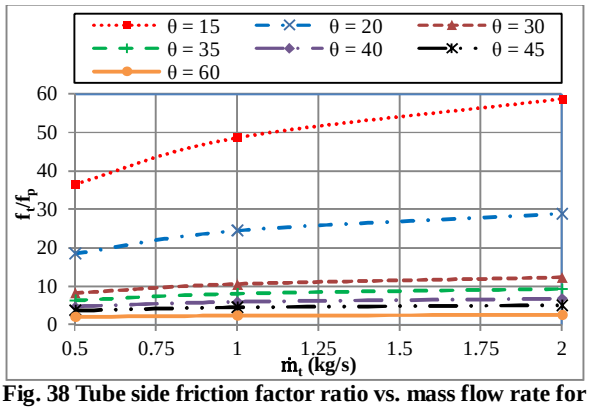

Fig. 38 Tube side friction factor ratio vs. mass flow rate for φ = 19 mm.

In case of fixed blade angle, the influence of using the inserted fixed vane swirlers in the inlet of the tube side with different vane swirlers diameter (φ = 5 mm, 10 mm, 15 mm and 19 mm) on friction factor for fixed blade angle of (θ = 15º, 30º, 45º and 60º) as follows:

For θ = 15º the friction factor increases significantly with the increase in vane swirlers diameter and the increase ratio increases with the increase in mass flow rate reaching its maximum value of friction factor of 58.8 times that of plain tube at φ = 19 mm, and the flow in this case are facing an almost total flow blockage although the heat transfer are found to be maximum also as shown in the following Figs. 39 and 40.

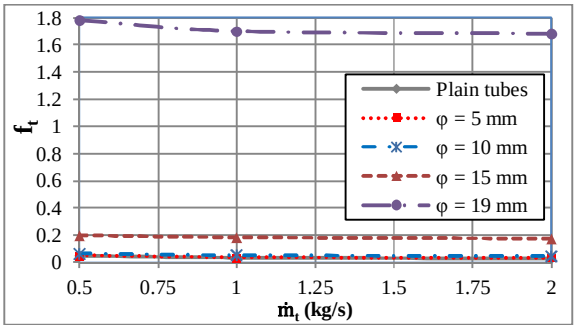

Fig. 39 Tube side friction factor vs. mass flow rate for θ = 15º.

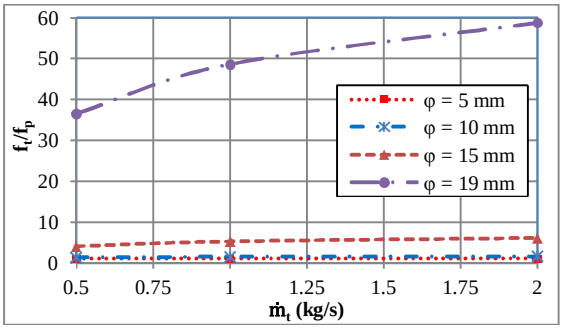

Fig. 40 Tube side friction factor ratio vs. mass flow rate for θ = 15º.

For θ = 30º, 45º and 60º friction factor increases significantly with the increase in vane swirlers diameter and the increase ratio increases with the increase in mass flow rate, as presented in the following Figs. 41 to 46, reaching its maximum values at φ = 19 mm, friction factor of 12.3, 5.0 and 2.5 times that of plain tube and this increase is found to be decreasing with the increase in blade angle as flow passage are less flow interrupted and thus less inertial flow.

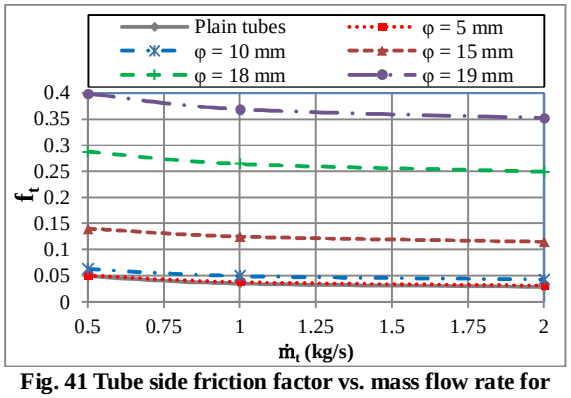

Fig. 41 Tube side friction factor vs. mass flow rate for θ = 30º.

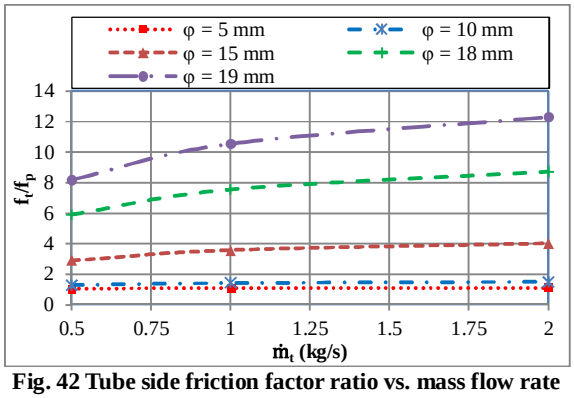

Fig. 42 Tube side friction factor ratio vs. mass flow rate for θ = 30º.

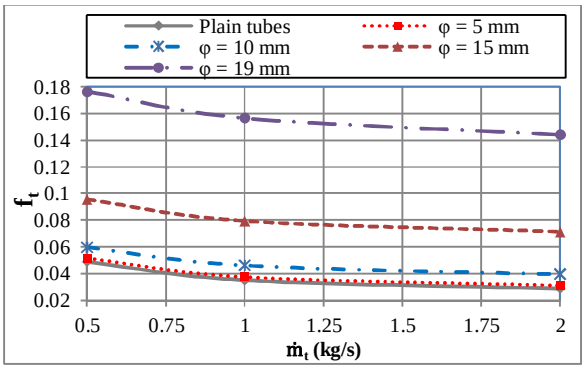

Fig. 43 Tube side friction factor vs. mass flow rate for θ = 45°.

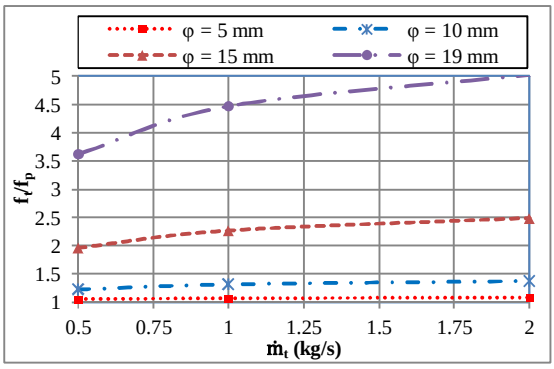

Fig. 44 Tube side friction factor ratio vs. mass flow rate for θ = 45°.

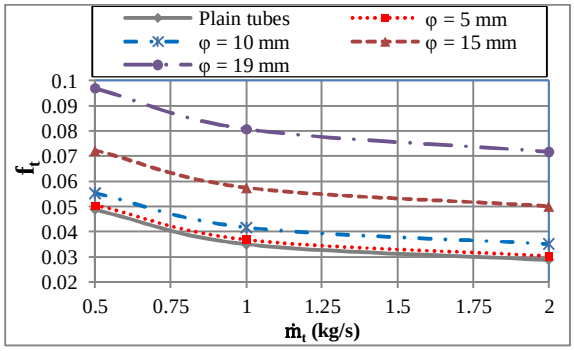

Fig. 45 Tube side friction factor vs. mass flow rate for θ = 60°.

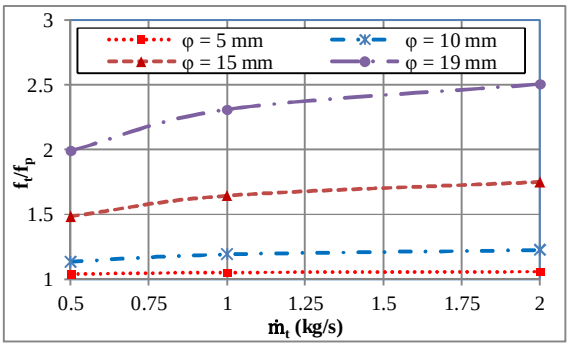

Fig. 46 Tube side friction factor ratio vs. mass flow rate for θ = 60°.

12.4 CORRELATION FOR SINGLE VANE SWIRLER PER EACH TUBE

The present predictions for Nusselt number and friction factor are presented in a correlation using regression method with standard deviation of 2.2%, and the correlation is as follows:

$$Nu = 0.2868 \frac{(1+\tan\theta)^{0.0296}\,\mathrm{Re}^{0.6187}\,f^{0.114}}{(D_b/D_p)^{0.0213}} \qquad (21)$$

Where the correlation range is θ = 15°, 30°, 45° and 60°, D_b/D_p = 0.25, 0.5, 0.75, 0.9 and 0.95, and Re = 5,000 – 21,000.

In case of fixed vane swirler diameter, the influence of using the inserted fixed vane swirlers in the inlet of the tube side with different blade angles (θ = 15°, 20°, 30°, 35°, 40°, 45° and 60°) on the relation between Nusselt number and friction factor for fixed vane swirlers diameter of (φ = 5 mm, 10 mm, 15 mm and 19 mm) are shown in the following Figs. 47 to 50, which are showing that the increase in Nusselt number decreases friction factor and this effect is decreased with the increase in vane swirlers diameter and the values for both are increased with the decrease in blade angle and the effect of blade angle are more significant with the increase in vane swirlers diameter.

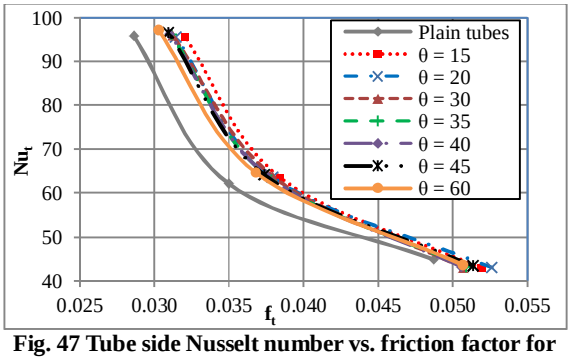

Fig. 47 Tube side Nusselt number vs. friction factor for φ = 5 mm.

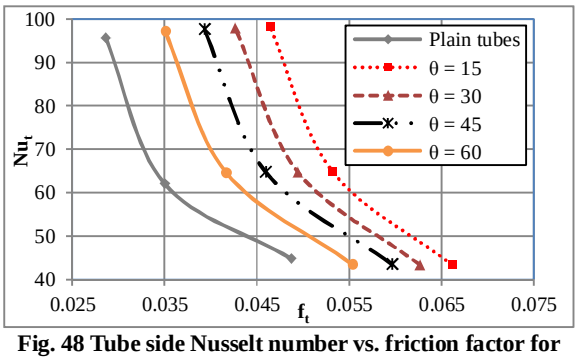

Fig. 48 Tube side Nusselt number vs. friction factor for φ = 10 mm.

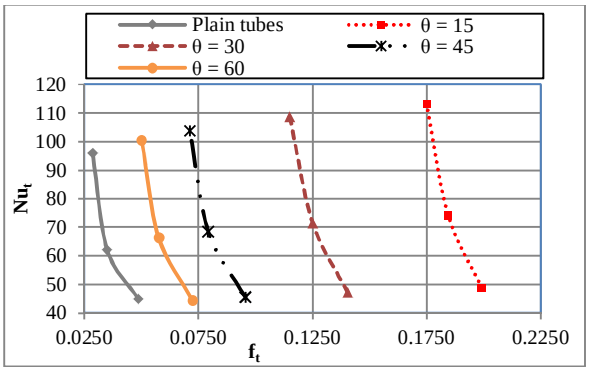

Fig. 49 Tube side Nusselt number vs. friction factor for φ = 15 mm.

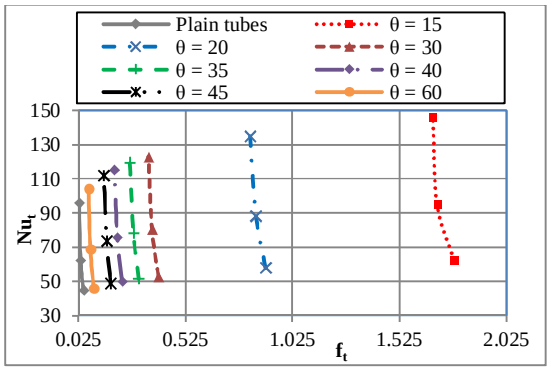

Fig. 50 Tube side Nusselt number vs. friction factor for φ = 19 mm.

In case of fixed blade angle, the influence of using the inserted fixed vane swirlers in the inlet of the tube side with different vane swirlers diameter (φ = 5 mm, 10 mm, 15 mm and 19 mm) on the relation between Nusselt number and friction factor for fixed blade angle of (θ = 15º, 30º, 45º and 60º) are shown in the following Figs. 51 to 54, which are showing that a small effect on the friction factor with the increase in Nusselt number at small blade angles and this effect is increasing with the increase in blade angle, while the friction factor increases significantly with the increase in vane swirlers diameter and a less increase in Nusselt number are found specially in small blade angles which means that at high vane swirlers diameter and small blade angle the main role is the fiction factor not the Nusselt number.

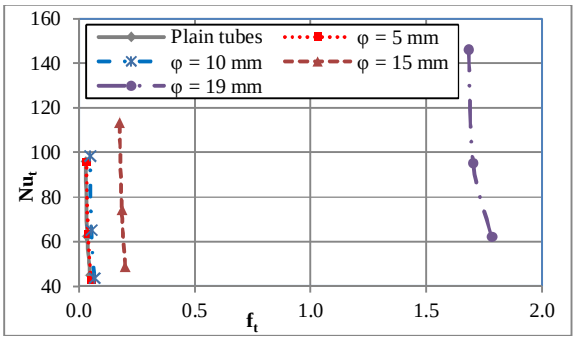

Fig. 51 Tube side Nusselt number vs. friction factor for θ = 15º.

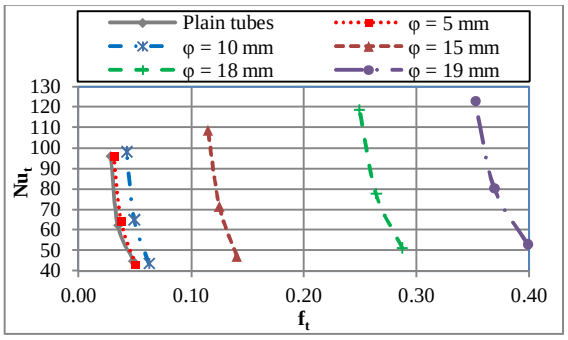

Fig. 52 Tube side Nusselt number vs. friction factor for θ = 30º.

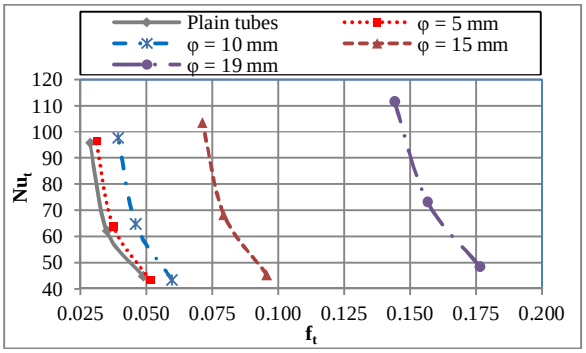

Fig. 53 Tube side Nusselt number vs. friction factor for θ = 45º.

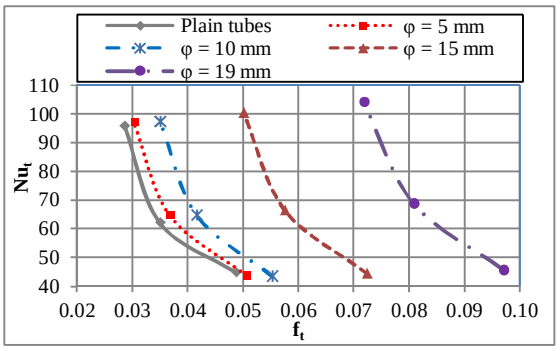

Fig. 54 Tube side Nusselt number vs. friction factor for θ = 60º.

12.5 COMPARISON WITH OTHERS' RESULTS FOR SINGLE VANE SWIRLER PER EACH TUBE

A comparison is made between the Kurtbus et al. [3] correlation, the present predictions, and correlation for the range that considerably close to Kurtbus et al. [3] correlation as shown in Figs. 55 to 57. The comparison show the same trend for relation curve between tube side Nusselt number and Reynolds number, also a perfect matching is found at (θ = 15º & φ = 15 mm) as in Fig. 55 which give a more confidence in both present predictions and the developed correlation.

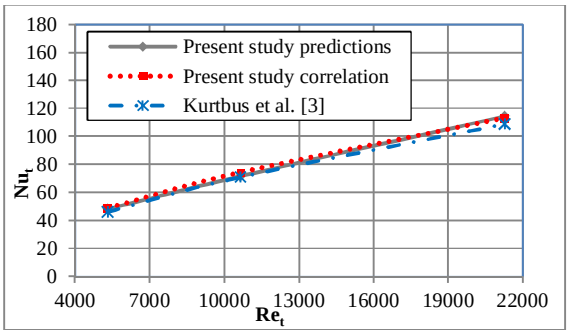

Fig. 55 Tube side Nusselt number vs. Reynolds number for θ = 15° and φ = 15 mm.

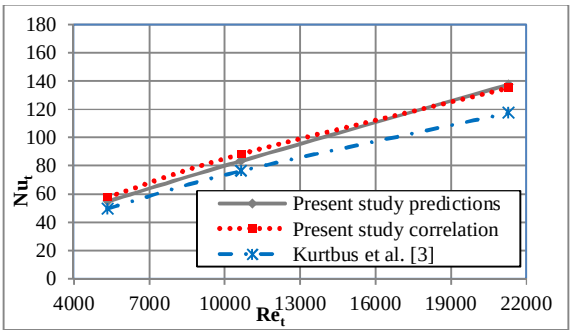

Fig. 56 Tube side Nusselt number vs. Reynolds number for θ = 20° and φ = 19 mm.

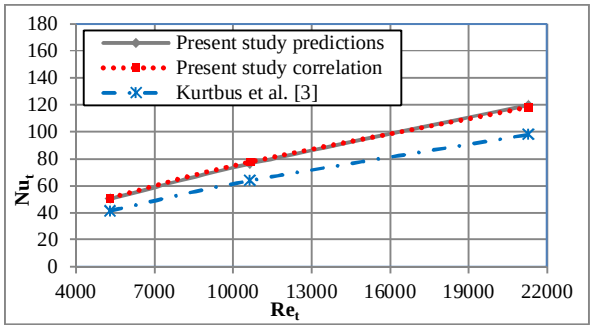

Fig. 57 Tube side Nusselt number vs. Reynolds number for θ = 30° and φ = 18 mm.

12.6 THERMAL ENHANCEMENT FACTOR FOR SINGLE VANE SWIRLER PER EACH TUBE

The evaluation of potential for real application of the inserted fixed vane swirlers as heat transfer enhancement device is performed using thermal enhancement factor. In general, friction factor ratio increases with increasing Reynolds number. Consequently, the effect of friction factor ratio becomes dominantly over the Nusselt number ratio at high Reynolds number (turbulent flow regime), resulting in thermal performance less than unity. On the other hand, the thermal enhancement factors above unity are found in low Reynolds number regime (laminar flow regime), indicating the potential of these inserted fixed vane swirlers as energy-saving devices as in all cases of swirling flow, the heat transfer increased at the expense of increased pressure drop.

In case of fixed vane swirler diameter, For φ = 5 mm the thermal enhancement factor is almost constant at 0.97 as in the following Fig. 58 due to Nusselt number equal to that of plain tube with no noticeable enhancement and friction factor slightly above that of plain tube.

For φ = 10, 15 and 19 mm as in the following Figs. 59 to 61 the thermal enhancement factor decreases as friction factor ratio increases with increasing in mass flow rate. Consequently, the effect of friction factor ratio becomes dominantly over the Nusselt number ratio at higher mass flow rate result in thermal enhancement factor less than unity, also thermal enhancement factor decreases with the decrease in blade angle reaching its minimum value at θ = 15° due to the increase in turbulence intensity which results in both increase in heat transfer and friction factor but with major increase in friction factor than that of heat transfer.

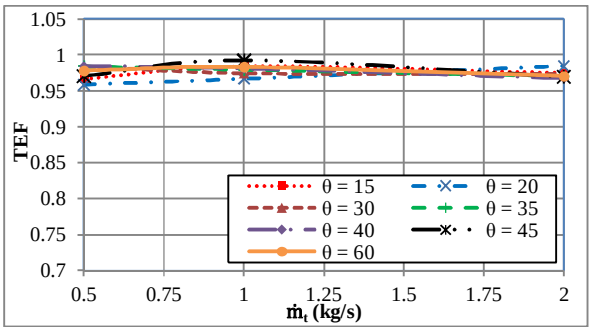

Fig. 58 Tube side thermal enhancement factor vs. mass flow rate for φ = 5 mm.

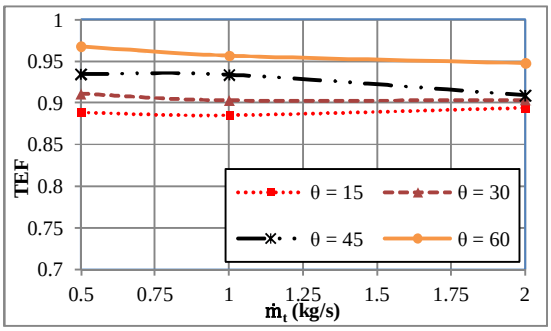

Fig. 59 Tube side thermal enhancement factor vs. mass flow rate for φ = 10 mm.

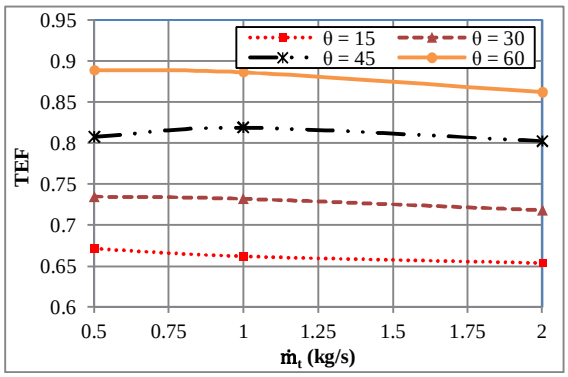

Fig. 60 Tube side thermal enhancement factor vs. mass flow rate for φ = 15 mm.

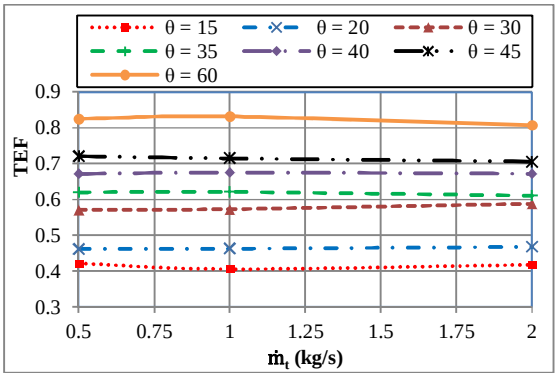

Fig. 61 Tube side thermal enhancement factor vs. mass flow rate for φ = 19 mm.

In case of fixed blade angle, the thermal enhancement factor in the following Figs. 62 to 65 decreases with the increase in mass flow rate, also decreases with the increase in vane swirlers diameter due to blockage effect of fluid flow which increases friction factor significantly more than the increase in heat transfer resulting a lower levels of thermal enhancement factor at φ = 19 mm.

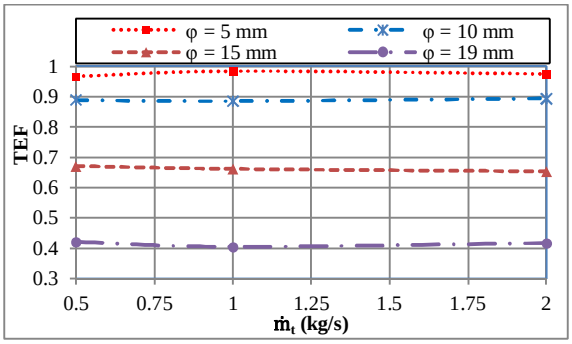

Fig. 62 Tube side thermal enhancement factor vs. mass flow rate for θ = 15°.

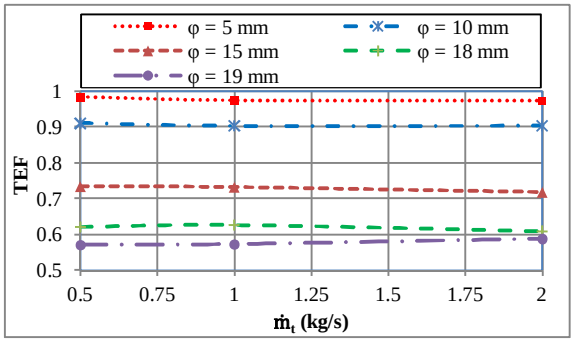

Fig. 63 Tube side thermal enhancement factor vs. mass flow rate for θ = 30°.

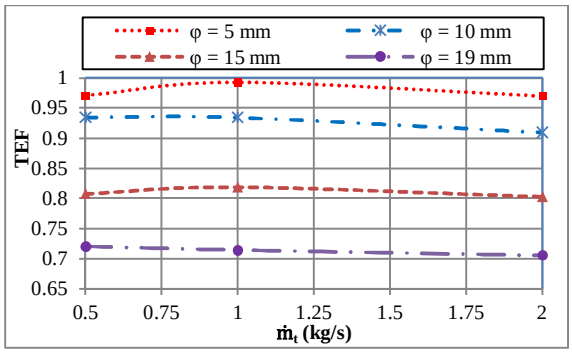

Fig. 64 Tube side thermal enhancement factor vs. mass flow rate for θ = 45°.

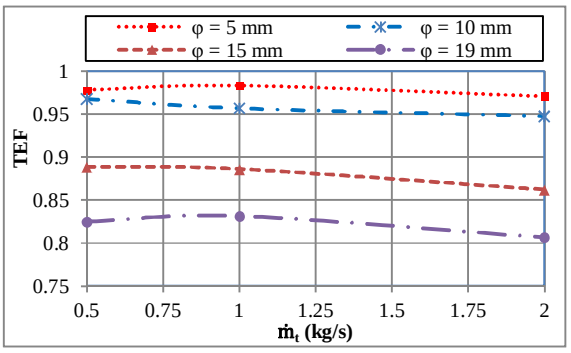

Fig. 65 Tube side thermal enhancement factor vs. mass flow rate for θ = 60°.

The swirl induced heat transfer enhancement which is unavoidably accompanied by friction loss in the tubes. The lower blade angle and higher vane swirlers diameter generates friction loss within the heat exchanger of unsatisfactory level, resulting in low thermal enhancement factor. So, the margin for selecting the proper vane swirler is the required heat transfer enhancement level with the maximum permissible friction loss.

13. CONCLUSIONS

1- Tube side Nusselt number predictions match with different correlations but deviates to a maximum percentage of 19.7% at high Reynolds number.

2- Tube side friction factor predictions deviation reaches in some cases 28.6% but still the predictions is considered satisfactory as it is laying between different correlations results.

3- Shell side heat transfer coefficient and pressure drop predictions deviation reaches in some cases 15.8% and 20% respectively, but still the predictions is considered satisfactory as it is laying between Ozden and Tari predictions and Bell-Delaware analytical method.

4- The insertion of fixed vane swirlers in the tube side; slightly affecting on the shell side Nusselt number and friction factor.

5- The increase in mass flow rate increases tube side Nusselt number while slightly decreases tube side friction factor and thermal enhancement factor.

6- The increase in inserted vane swirlers diameter with the decrease in blades angle; increases the tube side Nusselt number and friction factor, while decreases tube side thermal enhancement factor.

7- For single inserted vane swirlers; the highest achieved heat transfer enhancement is for φ = 19 mm and $\theta = 15^{o}$ case, resulting in for Nusselt number, friction factor, and thermal enhancement factor times that of plain tubes case of 1.62, 58.75, and 0.42, respectively.

REFERENCES

[1] Liang, C., and Papadakis, G., "Large Eddy Simulation of Cross-Flow through a Staggered Tube Bundle at Subcritical Reynolds Number", J. Fluids and Structures 23, 2007, pp. 1215 – 1230.

[2] Sobota, T., "Experimental prediction of heat transfer correlations in heat exchangers", Cracow University of Technology, Poland, Chapter 16 in: Development in Heat Transfer (M.A.S Bernades, ed.), In-Tech, Vienna – Rijeka, ISBN 978-953-307-569-3, 2011.

[3] Kurtbas, I., Durmus, A., Eren, H., and Turgut, E., "Effect of propeller type swirl generators on the entropy generation and efficiency of heat exchangers", Int. J. of Thermal Sciences, Vol. 46, Issue 3, 2007, pp. 300–307.

[4] Eiamsa–ard, S., Thianpong, C., Eiamsa-ard, P., and Promvonge, P., "Thermal characteristics in a heat exchanger tube fitted with dual twisted tape elements in tandem", J. Int. Communications in Heat and Mass Transfer, Vol. 37, Issue 1, 2010, pp. 39–46.

[5] Thianpong, C., Eiamsa-ard, P., Wongcharee, K., and Eiamsa-ard, S., "Compound heat transfer enhancement of a dimpled tube with a twisted tape swirl generator", J. International Communications in Heat and Mass Transfer 36, 2009, pp. 698–704.

[6] Blasius, H. Z., "The law of similar procedures in liquids friction", Researchers Arb. Ing. Wes., No. 131, Berlin, 1913.

[7] Petukhov, B.S., "Heat Transfer and Friction in Turbulent Pipe Flow with Variable Physical Properties". In: Irvine, T.F., Hartnett, J.P. (Eds.) Advances in Heat Transfer, vol. 6, 1970, Academic Press, New York, Cross Ref.

[8] Colburn, A.P., "A Method of Correlating Forced Convection Heat Transfer Data and a Comparison with Liquid Friction", Trans. AIChE 29, 1933, pp. 174–210.

[9] Winterton, R. H. S., "Where did the Dittus and Boelter equation come from?", Int. J. Heat Mass Transfer, Vol. 41, Nos. 4-5, 1998, pages 809–810.

[10] Bell, K. J., "Final Report of the Cooperative Research Program on Shell and Tube Heat Exchangers", Bull. No. 5, 1963, University of Delaware Engineering Experiment Station, New York.

[11] Col, D. D. Muzzolon, A., Piubello, P., and Rosetto, L., "Measurement and prediction of evaporator shell-side pressure drop", Int. J. Refrigeration, 28, 2005, pp. 320–330.

[12] Ozden, E., and Tari, I., "Shell Side CFD Analysis of a Small Shell–and–Tube Heat Exchanger", J. Energy Conversion and Management 51, 2010, pp. 1004 – 1014.

[13] Ur-Rehman, U., "Heat Transfer Optimization of Shell–and–Tube Heat Exchanger through CFD Studies", M.Sc. Thesis, 2011, Chalmers University of Technology, Göteborg, Sweden.

[14] ANSYS FLUENT Documentation, ANSYS, Inc., Release 15.0, 2013.

[15] Yehia, M. G., Attia, A. A. A., Abdelatif, O. S., and Khalil, E. E., "Computational Investigations of Thermal Simulation of Shell and Tube Heat Exchanger", ASME 2014 12th Biennial Conference on Engineering Systems Design and Analysis, ESDA2014, June 25-27, 2014, Copenhagen, Denmark.

[16] Incropera, F. P., DeWitt, D.P., Bergman, T.L., and Lavine, A.S., "Introduction to Heat Transfer", 6th Ed., 2011, John Wiley & Sons, Inc.

[17] Eiamsa–ard, S., and Promvonge, P., "Experimental investigation of heat transfer and friction characteristics in a circular tube fitted with V–nozzle turbulators", Int. Communications in Heat and Mass Transfer, Vol. 33, Issue 5, 2006, pp. 591–600.